Title

Reversible Electrochemical Interface of Mg Metal and Conventional Electrolyte Enabled by Intermediate Adsorption

Journal

ACS Energy Letters, 5(1)

ISSN

2380-8195

Authors

Wang, Hui
Feng, Xuefei
Chen, Ying
et al.

Publication Date

2020-01-10

DOI

10.1021/acsenergylett.9b02211

Reversible electrochemical interface of Mg metal and conventional electrolyte enabled by intermediate adsorption

Hui Wang[1,2], Xuefei Feng[2,3], Ying Chen[2,4], Yi-Sheng Liu[2,3], Kee Sung Han[2,4], Mingxia Zhou[2,5], Mark H. Engelhard[6], Vijayakumar Murugesan[2,4], Rajeev S. Assary[2,5], Tianbiao Leo Liu[1], Wesley Henderson[1], Zimin Nie[1], Meng Gu[6], Jie Xiao[1], Chongmin Wang[6], Kristin Persson[2,7,8], Donghai Mei[4], Ji-Guang Zhang[1], Karl T. Mueller[2,4], Jinghua Guo[2,3], Kevin Zavadil[2,9], Yuyan Shao[1,2]*, Jun Liu[1]

1. Energy & Environment Directorate, Pacific Northwest National Laboratory, Richland, Washington 99352, USA
2. Joint Center for Energy Storage Research (JCESR), Lemont Illinois 60439, USA.
3. Advanced Light Source, Lawrence Berkeley National Laboratory, Berkeley, California 94720, USA.
4. Physical and Computational Sciences Directorate, Pacific Northwest National Laboratory, Richland, Washington 99352, USA
5. Materials Science Division, Argonne National Laboratory, 9700 S. Cass Avenue, Illinois 60439, USA
6. Environmental Molecular Sciences Laboratory, Pacific Northwest National Laboratory, Richland, Washington 99352, USA
7. Energy Technologies Area, Lawrence Berkeley National Laboratory, Berkeley, California 94720, USA
8. Department of Materials Science and Engineering, University of California, Berkeley, Berkeley, California 94720, USA
9. Material, Physical, and Chemical Sciences, Sandia National Laboratories, Albuquerque, New Mexico 87185, USA.

Corresponding author: yuyan.shao@pnnl.gov

Abstract

Conventional electrolytes made by mixing simple Mg^{2+} salts and aprotic solvents, analogous to those in Li-ion batteries, are incompatible with Mg anodes because Mg metal readily reacts with such electrolytes, producing a passivation layer which blocks Mg^{2+} transport. Here, we report that, through tuning a conventional electrolyte—$Mg(TFSI)_2$ ($TFSI^-$ is $N(SO_2CF_3)_2^-$) with an $Mg(BH_4)_2$ additive, highly reversible Mg plating/stripping with a high coulombic efficiency is achieved, by neutralizing the first solvation shell of Mg cationic clusters between Mg^{2+} and $TFSI^-$ and enhanced reductive stability of free $TFSI^-$. A critical adsorption step between Mg^0 atoms and active Mg cation clusters involving BH_4^- anions is identified to be the key enabler for reversible Mg plating/stripping through analysis of distribution of relaxation times (DRT) from operando electrochemical impedance spectroscopy (EIS), operando electrochemical X-ray absorption spectroscopy (XAS), nuclear magnetic resonance (NMR), and density functional theory (DFT) calculations. This study suggests a new approach for developing advanced electrolytes for Mg batteries and provides a set of *in-operando* analysis tools for probing electrified Mg/electrolyte interfaces.

Introduction

The deployment of large-scale electric energy storage for transportation and electric grid applications stipulates the need for low cost, safe and high energy density battery technologies.[1-3] Magnesium batteries are one promising technology that could potentially meets these requirements because of the high volumetric capacity (for comparison: 3832 mAh/cm$^3_{Mg}$, 2062 mAh/cm$^3_{Li}$ and 1136 mAh/cm$^3_{Na}$), better safety (Mg metal anodes can be nondendritic [4, 5] and less chemically reactive than Li or Na metal), and low cost by using the earth abundant element Mg. Tremendous progress [6-13] has been made in the Mg battery field since the first prototype rechargeable Mg battery was reported by Aurbach and coworkers in 2000[14]. Still, significant technical challenges remain, including the limited performance and high incompatibility of electrolytes (with electrode materials), sluggish solid-state transfer kinetics of Mg^{2+} cations. In addition, limited fundamental understanding of Mg electrolyte/electrode interfaces presents a scientific challenge for design and development of better materials for Mg batteries (in stark contrast to Li-ion battery chemistry[15, 16]).

The properties of Mg-based electrolytes differ significantly from those for Li or Na batteries[17]. Conventional electrolytes made by mixing simple Mg^{2+} salts and solvents, analogous to those in Li-ion batteries[18], are not compatible with Mg metal anodes. It is widely reported that Mg deposition is difficult in conventional electrolytes[15, 19-21]. This is attributed to the solid electrolyte interfacial (SEI) layer formed on the Mg metal surface that does not permit the transport of the divalent Mg^{2+} [15, 22, 23]. Instead, special electrolytes are needed (e.g., with organometallic components) which require more complicated chemical synthesis/purification processes[15, 24]. To date, there are only a limited number of electrolytes which enable reversible Mg plating/stripping [7, 9, 25-29]. These electrolytes have notable limitations, such as the poor dissociation and conduction of Mg^{2+} [30], low electrochemical stability window (which severely restricts the cathodes that may be used and thus the energy density of the batteries)[7], corrosive characteristics and high volatility/flammability due to the use of solvents such as tetrahydrofuran (THF)[26, 31]. During the past several decades, extensive knowledge has been gained on the chemistry, properties and optimization of electrolytes for lithium batteries. If such electrolytes could be tuned to be compatible with Mg metal—enabling reversible Mg plating/stripping—it will significantly broaden the choices of electrode and electrolyte materials available for use, thus providing new opportunities in developing Mg-based batteries.

In this paper, we demonstrate that, through tuning a conventional electrolyte composition, i.e., $Mg(TFSI)_2$ ($TFSI^-$ is the bis(trifluoromethanesulfonyl)imide anion $N(SO_2CF_3)_2^-$) in diglyme with an $Mg(BH_4)_2$ additive, highly reversible Mg plating/stripping with close to 100% coulombic efficiency (CE) can be achieved by neutralizing the first solvation shell of Mg cationic clusters between Mg^{2+} and $TFSI^-$ and enhanced reductive stability of free $TFSI^-$, thus making it possible to use conventional electrolytes together with a Mg metal anode. Further, the charge-transfer reaction with adsorption of active Mg cation clusters involving BH_4^- has been identified by a set of *in-operando* analysis tools to be the key mechanism for reversible Mg plating/stripping in this electrolyte.

Results and Discussion

An *in-operando* analysis kit

The interfacial chemistry on Mg metal is complex. Elucidating the electrolyte-dependent reversible Mg plating/stripping on electrified interface is thus of pivotal importance to design and develop electrolytes[32, 33]. Adsorption of active intermediate Mg^+ clusters ($[MgX]^+$) has been identified to be a vital step for reversible Mg plating/stripping by *in-operando* electrochemical XAS[30, 34]. However, it is still hard to detect the $[M\text{---}Mg]_{ad}$ state (i.e. a transient charge-transfer reaction intermediate) by *in-operando* XAS during the charge-transfer reaction, i,e., $M+[MgX]_{ad}^+ + 2e^- \rightarrow [M\text{---}Mg]_{ad} + X^-$ (a key step of Mg plating) due to the faster diffusion rate of Mg adatoms on the substrate surface[30]. *In-operando* electrochemical impedance spectroscopy (EIS) has gained wide popularity as a non-destructive, sensitive and highly informative method to explore the interfaces between metal electrodes and liquid electrolytes, which is complementary to *in-operando* XAS, particularly for charge-transfer reactions involving the adsorption step of active redox species[35]. However, it is still debatable to distinguish electrochemical processes with comparable time constants from the complex impedance spectrum. Recently, a new method of distribution of relaxation times (DRT), based on analysis of the measured impedance spectrum, has been established to interpret the complex electrochemical process with a much higher resolution[36, 37]. Especially, DRT analysis is an effective method in unveiling the emergence of new electrochemical processes (e.g. new surface film at electrodes, new charge-transfer and new adsorption, etc.) at evolving electrified interfaces[38, 39]. An integrated *in-operando* method (**Fig. 1)** is then proposed to probe the electrified interface under Mg/electrolyte interface with/without $Mg(BH_4)_2$, where BH_4^- tunes the active intermediate Mg^+ cluster.

BH_4^--dictated reversible Mg electrochemistry.

Magnesium electrochemistry is first studied in the conventional electrolyte 0.2M $Mg(TFSI)_2$ in diglyme. **Fig. 2a** shows the cyclic voltammogram (CV) with a Pt working electrode in 0.2 M $Mg(TFSI)_2$/diglyme. A reduction peak occurs below -0.4V, with a small oxidation peak near 0.4 V and a larger oxidation peak near 2.0 V (vs. Mg). An electrochemical experiment was designed to identify these peaks. Mg metal was initially electrodeposited from an Mg electrolyte (it has been confirmed that only Mg^0 could be obtained[40]). The Mg^0 was then rinsed with diglyme and transferred to a cell with the 0.2 M $Mg(TFSI)_2$/diglyme electrolyte. The electrochemical stripping of the Mg^0 was carried out after holding the electrode in the electrolyte for certain period of time (0, 1 and 5 min, respectively). With increasing holding time, a dramatic decrease in the peak at 0.4 V is observed in **Supplementary Fig. 1a**. This decrease is clearly linked with the corresponding increase in the second peak at 2.0 V. It can be deduced from the peak evolution, peak potential and Mg electrochemistry in "Mg electrolytes" (i.e., other electrolyte formulations which do enable highly reversible Mg plating/stripping) that the first oxidation peak (0.4 V) is ascribed to the electrochemical dissolution of Mg^0 and the second peak (2.0 V) to the oxidation of reaction products formed from the limited reaction between Mg^0 and the electrolyte components (specifically the $TFSI^-$ anion, as we will discuss later); the reduction peak below -0.4 V (Fig. 1a) is due to the electrochemical deposition of Mg metal. It is thus clear that Mg^0 can be electrodeposited from the conventional electrolyte without an additive (see further information in the following physicochemical characterization). Once Mg^0 is formed, however, it rapidly reacts with the conventional electrolyte resulting in Mg reaction products which can only be oxidized at high overvoltage. The reaction(s) take(s) place on a time scale of minutes with an estimated $t_{1/2}$ of less than 30 seconds (**Supplementary Fig. 1a**). By controlling the reaction time, the Mg^0 that

has not reacted with the electrolyte could be electrochemically stripped at low potential (i.e., the peak noted at 0.4 V).

Further structural and chemical analyses were pursued to confirm the above postulation. powder XRD patterns (**Supplementary Fig. 2**) for the deposited material from the 0.2 M $Mg(TFSI)_2$/diglyme electrolyte identify the existence of Mg metal. An X-ray photoelectron spectroscopic (XPS) characterization of the Mg deposition reveals additional information (**Fig. 1b** and **Supplementary Fig. 3**). The broad Mg2p peak (actually two overlapping peaks in **Fig. 1c**) indicates a complicated chemistry at the Mg surface ("As is" sample) and in the bulk material (the "Sputtered" sample for which ~20 nm was removed through Ar^+ sputtering), which includes signals from both Mg^0 and Mg^{2+} compounds[41]. Significant amounts of F, S, O, C are also observed in the Mg deposition (**Supplementary Fig. 3**) and the atomic ratio of F/S (F/S = 1.0-1.5) calculated from high-resolution XPS (**Table S1**) differs significantly from that for $Mg(TFSI)_2$ (F/S = 3.0), indicating that the F and S are not simply from surface-absorbed $Mg(TFSI)_2$ salt, but rather from the decomposition products of the $TFSI^-$ anion. Previous studies[22] have shown that Mg metal reacts with conventional electrolyte components (as well as trace water and CO_2 in the electrolyte or glovebox) to form a surface film, and the composition of such films is similar to that on Li metal surfaces exposed to a similar environment, i.e., metal oxide, metal hydroxide, carbonate, fluoride, sulfide, and other metal compounds[42]. The exact composition of the surface film, however, is highly dependent upon the electrolyte composition. Therefore, both Mg^0 and Mg^{2+} compounds containing F, S, C, O coexist in the Mg deposition from the $Mg(TFSI)_2$/diglyme electrolyte with the data strongly suggesting that the Mg compounds largely originate from the reaction of the deposited Mg^0 with the $TFSI^-$ anions. The likely reason why these compounds are not evident in the XRD patterns is because they are amorphous (**Supplementary Fig. 2**). Notably, several studies [21, 43] have shown that ethers are stable with Mg metal and our previous work [40] also shows that diglyme is stable against decomposition at the Mg metal surface.

In contrast to these results, when small amounts of $Mg(BH_4)_2$ salt is added to the 0.2 M $Mg(TFSI)_2$/diglyme electrolyte, dramatic changes of the electrochemical stripping of Mg^0 occur (**Supplementary Fig. 1b**). Only the oxidation peak at low overpotential (0.4 V) is observed and this peak does not change with holding time in the electrolyte. This inspired us to further explore this system to understand the fundamental mechanisms underlying the change in behaviour from the pure $Mg(TFSI)_2$ system and the implications for rechargeable Mg batteries.

Based upon the above observations, we used $Mg(BH_4)_2$ as an additive to prepare a 0.4 M $Mg(TFSI)_2$-0.1 M $Mg(BH_4)_2$/diglyme electrolyte. **Fig. 2c** shows the cyclic voltammogram, where we observe highly reversible Mg plating/stripping and the coulombic efficiency (CE) is calculated to be 98.8%. The XRD pattern (**Supplementary Fig. 4**) shows that Mg metal was deposited and the SEM image of the surface (**Supplementary Fig. 4**) shows a smooth and dendrite-free Mg deposition morphology. The XPS analysis exhibits Mg peaks for the Mg deposition (**Fig. 2d**) and no Mg signal after stripping, indicating fully reversible Mg plating/stripping processes. No F, S, N, or B signals are observed on Mg deposition (**Supplementary Fig. 5**). The narrow peak for the high resolution XPS Mg2p peak (**Fig. 2d**) indicates a simple Mg composition, most of which is Mg^0 with little or no Mg^{2+} [41]; in drastic contrast to the observations in **Fig. 2b**. This confirms that, with the $Mg(BH_4)_2$ additive, Mg^0 does not react with and decompose the $TFSI^-$ anions present in the electrolyte.

To investigate the change of the chemical environment of bulk electrolytes by $Mg(BH_4)_2$ additive, solution-state ^1H, ^{13}C, ^{19}F, and ^{11}B NMR measurements were carried out to provide

molecular-level structural and dynamic information of diglyme, $TFSI^-$ and BH_4^-. As shown in **Fig. 2e-f**, by increasing $Mg(TFSI)_2$ concentration from 0.1 to 1 M, ^{13}C linewidth of the three carbon species in diglyme increases, indicating that the mobility of diglyme is significantly reduced due to its coordination to Mg^{2+} in solution. When 0.1 M $Mg(BH_4)_2$ is introduced to 0.4 M $MgTFSI_2$/diglyme, ^{13}C linewidth of all three carbon resonances drop dramatically, suggesting an enhancement in the diglyme mobility. ^1H NMR shows the same trend (**Supplementary Fig. 6**), a rapid decrease in ^1H spin-spin relaxation time (T_2) by increasing $Mg(TFSI)_2$ concentration and a remarkable increase with the addition of 0.1 M $Mg(BH_4)_2$, confirming the faster solvent motion enabled by $Mg(BH_4)_2$ additive. ^{19}F NMR spectra of 0.4 M $Mg(TFSI)_2$/diglyme and $Mg(TFSI)_2$-$Mg(BH_4)_2$/diglyme exhibit little change in chemical shift but a slight line broadening (reduced T_2) in the mixture, while ^{11}B NMR spectra of $Mg(BH_4)_2$/diglyme and $Mg(TFSI)_2$-$Mg(BH_4)_2$/diglyme display identical pentet B resonances centered at -42.23 and -42.28 ppm respectively, and also a slight line broadening in the mixture. Combined these observations with a previous ^{25}Mg NMR and computational modeling study on the same system [44], we have thus harvested a complete picture of the change in solvation structures and molecular dynamics by addition of $Mg(BH_4)_2$. Since $TFSI^-$ is a weakly coordinating anion, $MgTFSI_2$ is supposed to mostly dissociate at low concentrations (0.1 M), and form contact ion pair at a higher concentration (0.4 M) with the dominant solvation structure $[Mg(TFSI)^+(diglyme)_2]$ (**Supplementary Scheme 1**). Since two diglyme molecules are involved in the first solvation shell, solvent mobility decreases with Mg^{2+} concentration, especially for the terminal CH_3, due to the coordination between neighboring oxygen and Mg^{2+}. In contrast, BH_4^- is a much stronger coordinating ligand and forms stable ion association $[Mg(BH_4)_2(diglyme)]$ even at a very low concentration (0.01 M). In the mixture of 0.4 M $Mg(TFSI)_2$ and 0.1 M $Mg(BH_4)_2$, both $TFSI^-$ and BH_4^- anions maintain in the first solvation shell, as suggested by the unaltered ^{19}F and ^{11}B NMR. The significantly elevated solvent dynamics demonstrated by ^1H and ^{13}C NMR compared to the neat $Mg(TFSI)_2$ solution indicates the release of diglyme from the first solvation shell. This is consistent with the solvation structure $[Mg(BH_4)(TFSI)(diglyme)]$ obtained from ^{25}Mg NMR studies[44].

Adsorption of active Mg cation clusters with BH_4^-.

The chemical environment of Mg^{2+} is significantly changed by addition of BH_4^-; the first solvation shell of contact ion-pairs between Mg^{2+} and $TFSI^-$ is accordingly neutralized (**Scheme 1**), which significantly inhibits the reduction of $TFSI^-$ in the mono-cationic Mg clusters (i.e. $[Mg(TFSI)^+(DGM)_2]$) accessible to substrate during Mg plating[45]. However, the role of active Mg^+ clusters with BH_4^- in reversible Mg electrochemistry on electrified interface are still unknown.

Fig. 3a-b shows potential-dependent *in-operando* EIS evolution of the working electrode of Pt disk in three-electrode Swagelok-cell (**Supplementary Fig. 7**) using electrolytes with/without BH_4^-. As we have pointed out in the beginning, the adsorption step of key intermediates is critical for reversible Mg plating/stripping, here we try to identify the adsorption intermediates if any. *In-operando* EIS has been developed to identify the adsorption intermediates [35, 46]. For cell using electrolyte with BH_4^-, the impedance of Pt working electrode substantially increases upon the cathodic sweeping from 0 V to -0.10 V, then gradually decreases

from -0.10 V to -0.20 V, and then suddenly decreases at -0.25 V due to the Mg electrodeposition. Initial impedance increase is probably associated with the generation of negative-charged Pt surface to repel anions. The later gradual decrease likely originates from the continuous adsorption of active cationic clusters (e.g., $(MgBH_4)^+$; this step involves the repelling of $TFSI^-$ in neutralized solvation shells away from Pt working electrode) . However, a totally different scenario was observed for the cell using electrolytes without BH_4^-. No significant impedance change was observed in the full cathodic sweeping from 0 V to -0.20 V, indicating no occurrence of effective adsorption and bulk electrodeposition. To further confirm the adsorption step prior to the onset of Mg electrodeposition, *in-operando* potentiostatic XAS was performed at 0 V and -0.15 V for both electrolytes using the three-electrode home-made cell (**Supplementary Fig. 7**). **Fig. 3c** shows an obvious shift to the low-energy edge (i.e. to the energy of Mg metal) for the cell using electrolyte with BH_4^- but not for the cell using electrolyte without BH_4^- [33]. The shift should be largely associated with active Mg cation clusters involving BH_4^- absorbed at the interface of Pt and electrolytes before the onset Mg electrodeposition. Similar shift was observed in other electrolytes that contain Mg adsorption intermediates to enable reversible Mg plating/stripping [30, 33]. Further, the adsorption of active Mg cation clusters involving BH_4^- was demonstrated, after Mg bulk electrodeposition, by the presence of an inductive loop for the Cu working electrode (**Supplementary Fig. 7**) in the lower frequency range of 1-0.01 Hz in **Fig. 3d** [35]**.** The proposed electrical equivalent circuit is often used to model the faradic reactions with one adsorption species and the fitted spectrum is pretty close to that of the raw one, indicating the rationality and validity of this electrical equivalent circuit [35]. Besides, preliminary periodic density functional theory calculations (**Supplementary Fig. 8**) indicate a thermodynamically favorable coordination interaction between BH_4^- and Mg surface compared to $TFSI^-$.

Adsorption-dependent non-passivation

In-operando EIS evolution of galvanostatic electrodeposited Mg onto Cu was recorded during OCV resting period at 0.5 mA cm^{-2} every hour in 0.4 M $Mg(TFSI)_2$+0.1M $Mg(BH_4)_2$/diglyme in **Fig. 4**. The inductive loop was always observed in the low frequency range (1-0.01 Hz) during the steady galvanostatic Mg electrodeposition, indicating the sustainable presence of an adsorption (R_{ads}) by intermediate active Mg cation clusters[35]. The first loop in the high frequency range is associated with the charge-transfer process (R_{ct}), which evolved into a steady state when the cell potential reached *ca.*-0.18 V. Postmortem analysis of corresponding DRT spectra show peaks for R_{ct} in the high frequency range (i.e. 10^4 Hz-10^2 Hz) and for R_{ads} in the middle-low frequency range (i.e. 10 Hz-0.01 Hz), which align well with the proposed electrical equivalent circuit in **Fig.3d**. DRT results also clearly present the evolving interface in details, without the fitting process, in terms of the evolution of the charge-transfer process (i.e. from R_{ct_Cu} to $R_{ct\_Mg}{}^0$) and the emergence of a new adsorption step ($R_{ads\_Mg}{}^0$). Both new peaks are associated with newly-formed Mg electrodeposits onto Cu substrate. Especially, the charge-transfer reaction with the adsorption step of active Mg clusters onto Mg electrodeposits is uncovered by the DRT analysis.

However, **Supplementary Fig. 9** shows a totally different scenario for the cell without addition of $Mg(BH_4)_2$. Galvanostatic electrodeposition Mg onto Cu is terminated by the passivation with the emergence of the second large semicircle in the middle-low frequency range (10-0.1 Hz) and an inclined line ($R_{warburg\_Mg}{}^0$; 0.1-0.01 Hz), which can be explained by the modified Randle-circuit. DRT analysis suggests that the charge-transfer process ($R_{ct\_Mg}{}^0$) is a dominant electrochemical process at *ca.* 10 Hz and the migration of Mg^{2+} toward this surface

film (i.e $R_{SEI\_Mg^0}$) is sluggish which is revealed by the peak positioned at a middle frequency of *ca.* 400 Hz, analogous to the reported typical frequency range for SEI (1 kHz to 10 Hz) and for charge-transfer process (10 Hz to mHz) in Li-ion batteries [36] . It is thus concluded that non-passivation is driven by the adsorption of active Mg cation clusters with BH_4^-.

In summary, we have shown that—with a specific additive, i.e., $Mg(BH_4)_2$— a conventional electrolyte such as $Mg(TFSI)_2$/diglyme, which is not stable against Mg metal in itself, can be tuned to enable reversible Mg plating/stripping with high coulombic efficiency, permitting the use of this electrolyte for rechargeable Mg battery applications. We propose that the stronger interaction between Mg^0, Mg^{2+} and BH_4^- (as compared to $TFSI^-$) results in a preferred absorption (but not decomposition) of the BH_4^- anions on the Mg metal surface during the charge-transfer reaction. This in turn prevents undesirable side reactions between the Mg^0 and passivating Mg cationic clusters with $TFSI^-$, thus allowing highly reversible Mg plating/stripping. This adsorption mechanism may plausibly be extended to other electrolyte compositions, thus providing direct guidance for Mg battery development.

Acknowledgement

This work was supported as part of the Joint Center for Energy Storage Research (JCESR), an Energy Innovation Hub funded by the U.S. Department of Energy (DOE), Office of Science, Basic Energy Sciences. The XPS/SEM were performed at the Environmental Molecular Sciences Laboratory (EMSL), a national scientific user facility sponsored by the DOE Office of Biological and Environmental Research and located at Pacific Northwest National Laboratory (PNNL). The operando XAS work at Advanced Light Source of Lawrence Berkeley National Laboratory (LBNL) was supported by the Director of the Office of Science, Office of Basic Energy Sciences, of DOE under contract no. DEAC02-05CH11231.We gratefully acknowledge the computing resources provided on "BEBOP", a computing cluster operated by the Laboratory Computing Resource Center at Argonne National Laboratory (ANL).

Author Contributions

Y.Y. S. and H. W. conceived and designed the experiments. Y. Y. S. developed electrolyte formulations and performed CV measurements. H.W. carried out *in operando* EIS measurements and DRT analysis. X.F.F., Y-S. L., and J.H. G. performed *in operando* XAS measurements. M. H. E conduted XPS measurements. Y.C., K. S. H. And T. L. L. performed NMR tests. M.X. Z and R.S. A computed DFT calculations. H. W. and Y.Y. S. wrote the manuscript. All authors discussed the results and reviewed the manuscript.

1. Dunn B, Kamath H, Tarascon J-M. Electrical Energy Storage for the Grid: A Battery of Choices. *Science* **334**, 928-935 (2011).

2. Yang Z, *et al.* Electrochemical Energy Storage for Green Grid. *Chem Rev* **111**, 3577-3613 (2011).

3. Liu J, *et al.* Materials Science and Materials Chemistry for Large Scale Electrochemical Energy Storage: From Transportation to Electrical Grid. *Adv Funct Mater* **23**, 929-946 (2013).

4. Matsui M. Study on electrochemically deposited Mg metal. *J Power Sources* **196**, 7048-7055 (2011).

5. Ling C, Banerjee D, Matsui M. Study of the electrochemical deposition of Mg in the atomic level: Why it prefers the non-dendritic morphology. *Electrochim Acta* **76**, 270-274 (2012).

6. Rajput NN, Seguin TJ, Wood BM, Qu X, Persson KA. Elucidating Solvation Structures for Rational Design of Multivalent Electrolytes—A Review. *Top Curr Chem* **376**, 19 (2018).

7. Muldoon J, Bucur CB, Gregory T. Quest for Nonaqueous Multivalent Secondary Batteries: Magnesium and Beyond. *Chem Rev* **114**, 11683-11720 (2014).

8. Canepa P, *et al.* Odyssey of Multivalent Cathode Materials: Open Questions and Future Challenges. *Chem Rev* **117**, 4287-4341 (2017).

9. Mao M, Gao T, Hou S, Wang C. A critical review of cathodes for rechargeable Mg batteries. *Chem Soc Rev* **47**, 8804-8841 (2018).

10. Hahn NT, *et al.* Enhanced Stability of the Carba-closo-dodecaborate Anion for High-Voltage Battery Electrolytes through Rational Design. *J Am Chem Soc* **140**, 11076-11084 (2018).

11. Luo J, Bi Y, Zhang L, Zhang X, Liu TL. A Stable, Non-corrosive Perfluorinated Pinacolatoborate Mg Electrolyte for Rechargeable Mg Batteries. *Angew Chem, Int Ed* **0**, (2019).

12. Du A, *et al.* An efficient organic magnesium borate-based electrolyte with non-nucleophilic characteristics for magnesium–sulfur battery. *Energy Environ Sci* **10**, 2616-2625 (2017).

13. Yoo HD, *et al.* Fast kinetics of magnesium monochloride cations in interlayer-expanded titanium disulfide for magnesium rechargeable batteries. *Nat Commun* **8**, 339 (2017).

14. Aurbach D, *et al.* Prototype systems for rechargeable magnesium batteries. *Nature* **407**, 724 (2000).

15. Aurbach D, Schechter A, Moshkovich M, Cohen Y. On the Mechanisms of Reversible Magnesium Deposition Processes. *J Electrochem Soc* **148**, A1004-A1014 (2001).

16. Gershinsky G, Yoo HD, Gofer Y, Aurbach D. Electrochemical and Spectroscopic Analysis of Mg2+ Intercalation into Thin Film Electrodes of Layered Oxides: V2O5 and MoO3. *Langmuir* **29**, 10964-10972 (2013).

17. Borodin O, *et al.* Insights into the Structure and Transport of the Lithium, Sodium, Magnesium, and Zinc Bis(trifluoromethansulfonyl)imide Salts in Ionic Liquids. *J Phys Chem C* **122**, 20108-20121 (2018).

18. Xu K. Nonaqueous Liquid Electrolytes for Lithium-Based Rechargeable Batteries. *Chem Rev* **104**, 4303-4418 (2004).

19. Connor JH, Reid WE, Wood GB. Electrodeposition of Metals from Organic Solutions: V . Electrodeposition of Magnesium and Magnesium Alloys. *J Electrochem Soc* **104**, 38-41 (1957).

20. Genders JD, Pletcher D. Studies using microelectrodes of the Mg(II)/Mg couple in tetrahydrofuran and propylene carbonate. *J Electroanal Chem Interfacial Electrochem* **199**, 93-100 (1986).

21. Lu Z, Schechter A, Moshkovich M, Aurbach D. On the electrochemical behavior of magnesium electrodes in polar aprotic electrolyte solutions. *J Electroanal Chem* **466**, 203-217 (1999).

22. Aurbach D, *et al.* A short review on the comparison between Li battery systems and rechargeable magnesium battery technology. *J Power Sources* **97-98**, 28-32 (2001).

23. Hattori M, *et al.* Role of Coordination Structure of Magnesium Ions on Charge and Discharge Behavior of Magnesium Alloy Electrode. *J Phys Chem C* **122**, 25204-25210 (2018).

24. Muldoon J, *et al.* Electrolyte roadblocks to a magnesium rechargeable battery. *Energy Environ Sci* **5**, 5941-5950 (2012).

25. Mizrahi O, *et al.* Electrolyte Solutions with a Wide Electrochemical Window for Rechargeable Magnesium Batteries. *J Electrochem Soc* **155**, A103-A109 (2008).

26. Guo Y-s, Zhang F, Yang J, Wang F-f, NuLi Y, Hirano S-i. Boron-based electrolyte solutions with wide electrochemical windows for rechargeable magnesium batteries. *Energy Environ Sci* **5**, 9100-9106 (2012).

27. Kim HS, *et al.* Structure and compatibility of a magnesium electrolyte with a sulphur cathode. *Nat Commun* **2**, 427 (2011).

28. Gao X, *et al.* Prototype rechargeable magnesium batteries using ionic liquid electrolytes. *J Power Sources* **423**, 52-59 (2019).

29. Barile CJ, Barile EC, Zavadil KR, Nuzzo RG, Gewirth AA. Electrolytic Conditioning of a Magnesium Aluminum Chloride Complex for Reversible Magnesium Deposition. *J Phys Chem C* **118**, 27623-27630 (2014).

30. Benmayza A, *et al.* Effect of Electrolytic Properties of a Magnesium Organohaloaluminate Electrolyte on Magnesium Deposition. *J Phys Chem C* **117**, 26881-26888 (2013).

31. Pour N, Gofer Y, Major DT, Aurbach D. Structural Analysis of Electrolyte Solutions for Rechargeable Mg Batteries by Stereoscopic Means and DFT Calculations. *J Am Chem Soc* **133**, 6270-6278 (2011).

32. Ta K, See KA, Gewirth AA. Elucidating Zn and Mg Electrodeposition Mechanisms in Nonaqueous Electrolytes for Next-Generation Metal Batteries. *The Journal of Physical Chemistry C* **122**, 13790-13796 (2018).

33. Arthur TS, Glans P-A, Matsui M, Zhang R, Ma B, Guo J. Mg deposition observed by in situ electrochemical Mg K-edge X-ray absorption spectroscopy. *Electrochem Commun* **24**, 43-46 (2012).

34. Ye Y, Wu CH, Zhang L, Liu Y-S, Glans-Suzuki P-A, Guo J. Using soft x-ray absorption spectroscopy to characterize electrode/electrolyte interfaces in-situ and operando. *J Electron Spectros Relat Phenomena* **221**, 2-9 (2017).

35. Lasia A. Impedance of the Faradaic Reactions in the Presence of Adsorption. In: *Electrochemical Impedance Spectroscopy and its Applications* (ed^(eds). Springer New York Heidelberg Dordrecht London (2014).

36. Steinhauer M, Risse S, Wagner N, Friedrich KA. Investigation of the Solid Electrolyte Interphase Formation at Graphite Anodes in Lithium-Ion Batteries with Electrochemical Impedance Spectroscopy. *Electrochim Acta* **228**, 652-658 (2017).

37. Heinzmann M, Weber A, Ivers-Tiffée E. Advanced impedance study of polymer electrolyte membrane single cells by means of distribution of relaxation times. *J Power Sources* **402**, 24-33 (2018).

38. Ivers T, Eacute, E E, Weber A, eacute. Evaluation of electrochemical impedance spectra by the distribution of relaxation times. *Journal of the Ceramic Society of Japan* **125**, 193-201 (2017).

39. Weiß A, Schindler S, Galbiati S, Danzer MA, Zeis R. Distribution of Relaxation Times Analysis of High-Temperature PEM Fuel Cell Impedance Spectra. *Electrochim Acta* **230**, 391-398 (2017).

40. Shao Y, *et al*. Coordination Chemistry in magnesium battery electrolytes: how ligands affect their performance. *Sci Rep* **3**, 3130 (2013).

41. Ardizzone S, Bianchi CL, Fadoni M, Vercelli B. Magnesium salts and oxide: an XPS overview. *Appl Surf Sci* **119**, 253-259 (1997).

42. Aravindan V, Gnanaraj J, Madhavi S, Liu H-K. Lithium-Ion Conducting Electrolyte Salts for Lithium Batteries. *Chem Eur J* **17**, 14326-14346 (2011).

43. Aurbach D, *et al*. A comparison between the electrochemical behavior of reversible magnesium and lithium electrodes. *J Power Sources* **97-98**, 269-273 (2001).

44. Hu JZ, *et al*. 25Mg NMR and computational modeling studies of the solvation structures and molecular dynamics in magnesium based liquid electrolytes. *Nano Energy* **46**, 436-446 (2018).

45. Rajput NN, Qu X, Sa N, Burrell AK, Persson KA. The Coupling between Stability and Ion Pair Formation in Magnesium Electrolytes from First-Principles Quantum Mechanics and Classical Molecular Dynamics. *J Am Chem Soc* **137**, 3411-3420 (2015).

46. Liu Y, Wang W. Investigation on the Cu(II) and Co(II) Electrochemical Reduction Process in Citrate Solution by CV and EIS. *J Electrochem Soc* **159**, D375-D381 (2012).

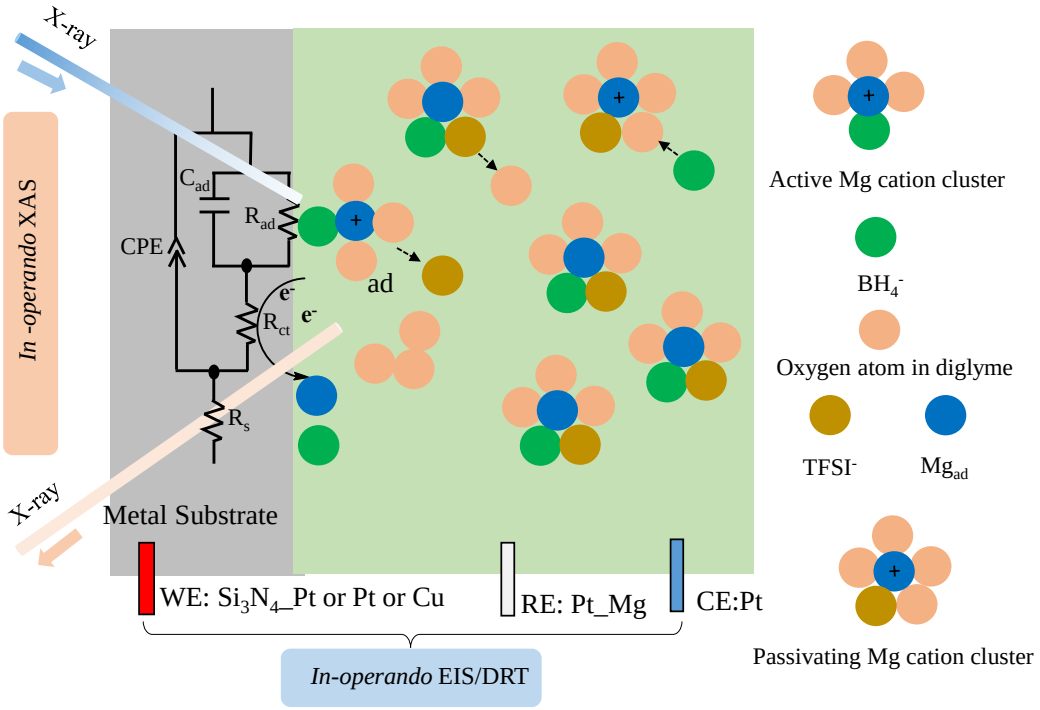

Figure 1 | Schematic illustration of probing the electrified interface involving adsorption of active Mg cation clusters. Mystery roles of Mg cation clusters at electrified interface are demonstrated to be uncovered by a coupled method of *in-operando* soft X-ray adsorption spectroscopy (XAS) and electrochemical impedance spectroscopy (EIS) and corresponding distribution of relaxation times (DRT) analysis. Typical conventional Mg electrolytes (i.e. $Mg(N(CF_3SO_2)_2$-in-diglyme), with/without additive of $Mg(BH_4)_2$, are developed to correlate the solvate composition with potential-dependent Mg plating/stripping reactivity.

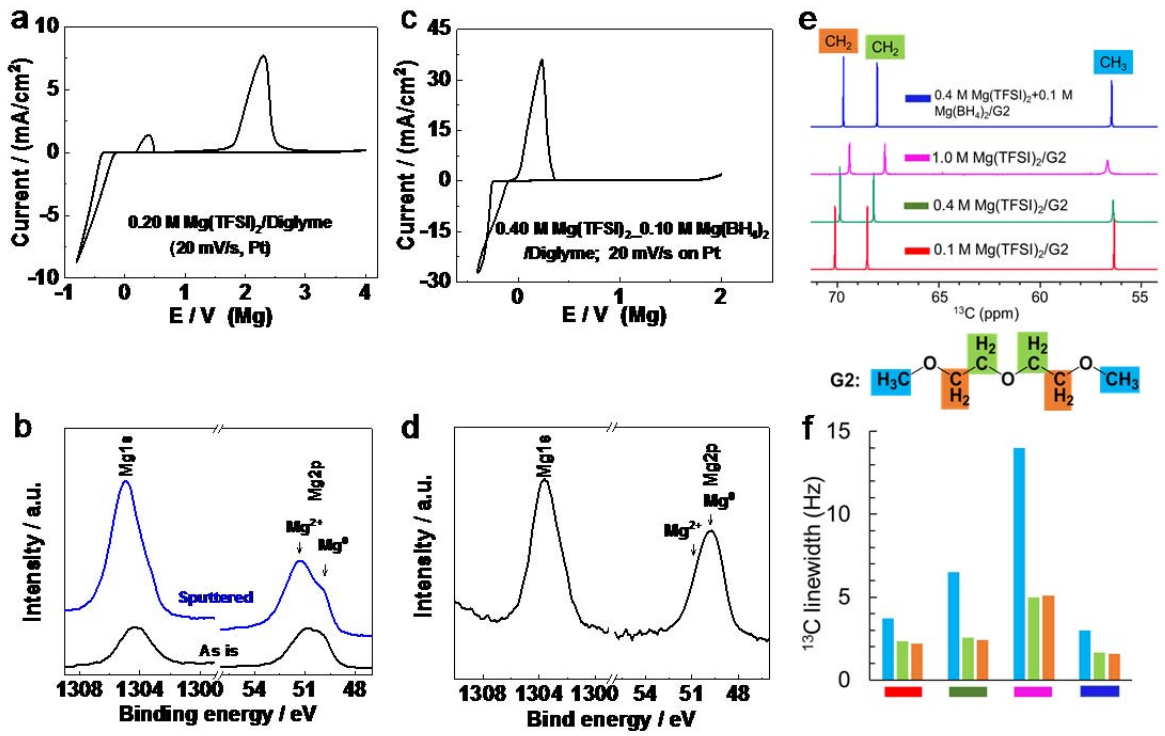

Figure 2 | BH_4^--dictated reversible Mg electrochemistry. a) CV (20 mV/s on Pt) in 0.2 M $Mg(TFSI)_2$/diglyme; b) XPS patterns of the Mg deposition from 0.2 M $Mg(TFSI)_2$/diglyme; c) CV (20 mV/s on Pt) in 0.4 M $Mg(TFSI)_2$+0.1 M $Mg(BH_4)_2$/diglyme; d) XPS patterns of the Mg deposition of the Mg deposition from 0.4 M $Mg(TFSI)_2$+0.1 M $Mg(BH_4)_2$/diglyme; e) ^{13}C NMR spectra and (f) the linewidth of three carbon resonances of diglyme with $Mg(TFSI)_2$ concentration varying from 0.1 to 1 M without and with 0.1 M $Mg(BH_4)_2$ additive

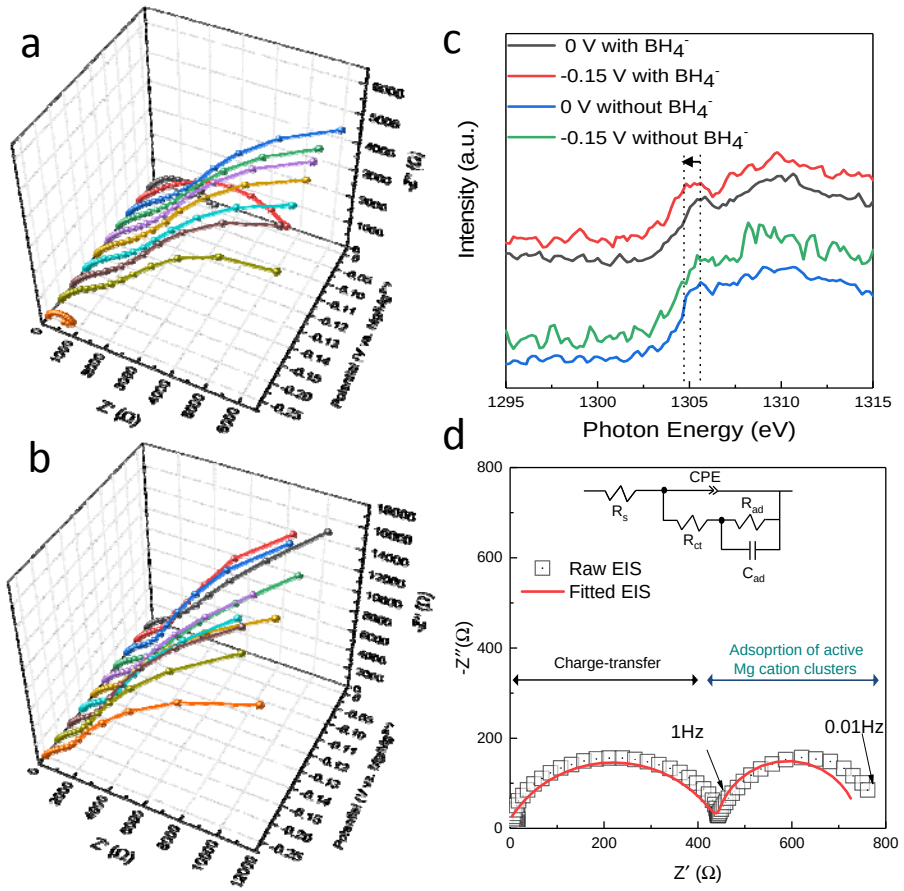

Figure 3 | Evidences on the adsorption of active Mg cation clusters with BH_4^-. Potential-dependent impedance evolution of the working electrode of Pt disk in three-electrode Swagelok-cell (Pt: WE; Mg: RE; Mg: CE) using 0.4 M $Mg(TFSI)_2$+0.1 M $Mg(BH_4)_2$/diglyme (a) and 0.4 M $Mg(TFSI)_2$/diglyme (b); (c) Pre-edge evolution of X-ray absorption near-edge spectroscopy (XANES) region of the Mg K-edge upon the cathodic sweeping from 0 V to -0.15 V (i.e. prior to the onset Mg electrodeposition) between the interface of Pt and 0.4M $Mg(TFSI)_2$+0.1M $Mg(BH_4)_2$/diglyme or 0.4M $Mg(TFSI)_2$/diglyme; (d) A typical impedance spectrum and corresponding fitted one with an inductive loop in the lower frequency range using electrolyte with $Mg(BH_4)_2$ after Mg bulk electrodeposition. The proposed electrical equivalent circuit is a typical one for impedance of the faradic reactions in the presence of one adsorption species.

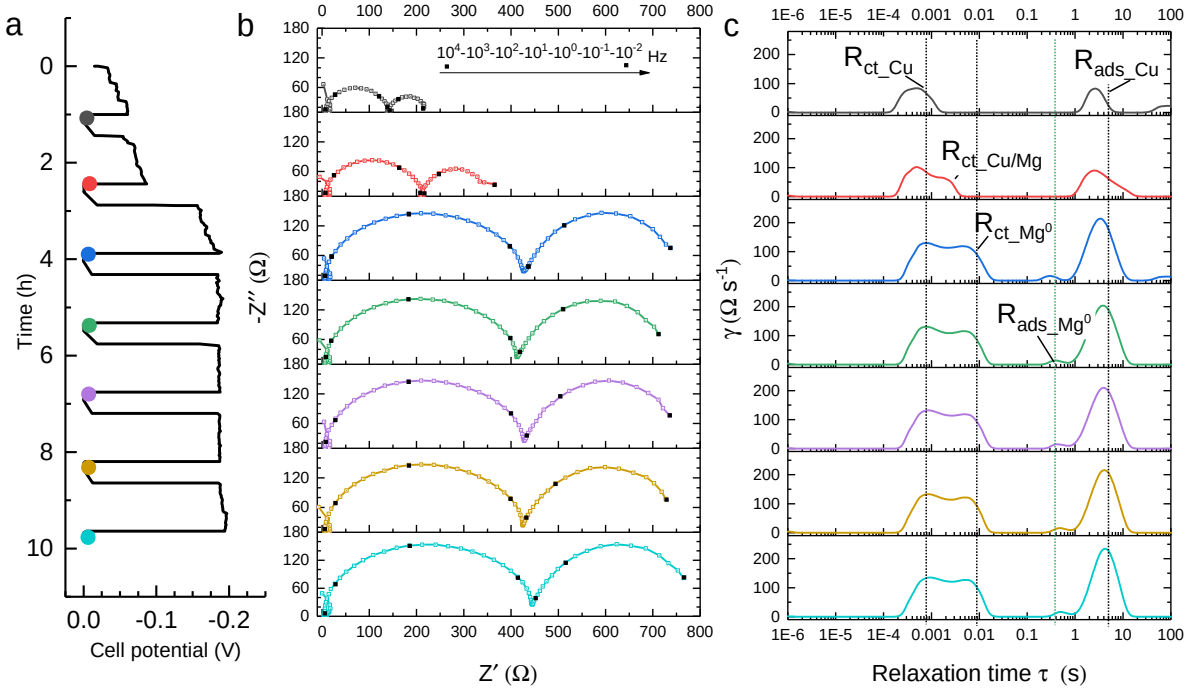

Figure 4 | Adsorption-dependent non-passivation. *In-operando* EIS evolution and corresponding analysis of DRT upon galvanostatic electrodeposited Mg onto Cu at 0.5 mA cm^{-2} in 0.4M $Mg(TFSI)_2$+0.1M $Mg(BH_4)_2$/diglyme. a) Discharge cell potential vs. time curve; b) evolution of recorded impedance spectra in the frequency range of 10^6-0.01 Hz; c) corresponding DRT spectra.